Time-Dependent Analysis of Catalytic Biomass Pyrolysis in a Continuous Drop Tube Reactor: Evaluating HZSM-5 Stability and Product Evolution

Chetna Mohabeer, Zineb Boutamine, Lokmane Abdelouahed, Antoinette Maarawi, Bechara Taouk

biomass

MDPI

Article

Time-Dependent Analysis of Catalytic Biomass Pyrolysis in a Continuous Drop Tube Reactor: Evaluating HZSM-5 Stability and Product Evolution †

Chetna Mohabeer [1], Zineb Boutamine [2], Lokmane Abdelouahed [1,*], Antoinette Maarawi [1] and Bechara Taouk [1]

[1] INSA Rouen Normandie, University Rouen Normandie, UNIROUEN, Laboratoire de Sécurité des Procédés Chimiques LSPC EA-4704, 76000 Rouen, France; chikirsha.mohabeer@insa-rouen.fr (C.M.); antoinette.maarawi@insa-rouen.fr (A.M.); bechrara.taouk@insa-rouen.fr (B.T.)

[2] Laboratory of Process Engineering for Sustainable Development and Health Products, Ecole Nationale Polytechnique de Constantine, Constantine 25000, Algeria; zaineb.boutamine@enp-constantine.dz

* Correspondence: lokmane.abdelouahed@insa-rouen.fr

† This paper is a part of the Ph.D. Thesis of Chetna Mohabeer, presented at INSA Rouen, France in the front matter.

Abstract: This study investigates a continuous deoxygenation of bio-oil vapor in a catalytic fixed-bed reactor coupled to a continuous drop tube reactor (DTR) for biomass pyrolysis. Beech wood pyrolysis was initially examined without catalysts at various temperatures (500–600 °C). The products were characterised using GC-MS, Karl Fischer titration, GC-FID/TCD, and thermogravimetric analysis. The highest bio-oil yield (58.8 wt.%) was achieved at 500 °C with a 500 mL/min N_2 flow rate. Subsequently, ex situ catalytic pyrolysis was performed using an HZSM-5 catalyst in a fixed-bed reactor at a DTR outlet, operating at 425 °C, 450 °C, and 500 °C. The HZSM-5 catalyst exhibited declining deoxygenation efficiency over time, which was evidenced by decreasing conversion rates of chemical families. Principal component analysis was employed to interpret the complex dataset, facilitating a visualisation of the relationships between the experimental conditions and product compositions. This study highlights the challenges of continuous operation as experimental durations were limited to 120 min due to clogging issues. This research contributes to understanding continuous biomass pyrolysis coupled with catalytic deoxygenation, providing insights into the reactor configuration, process parameters, and catalyst performance crucial for developing efficient and sustainable biofuel production processes.

Keywords: continuous pyrolysis; beech wood; drop tube reactor; fixed-bed catalytic reactor; deoxygenation treatment; HZSM-5

Citation: Mohabeer, C.; Boutamine, Z.; Abdelouahed, L.; Maarawi, A.; Taouk, B. Time-Dependent Analysis of Catalytic Biomass Pyrolysis in a Continuous Drop Tube Reactor: Evaluating HZSM-5 Stability and Product Evolution. *Biomass* **2024**, *4*, 1238–1256. https://doi.org/10.3390/biomass4040069

Academic Editor: Jaehoon Kim

Received: 21 October 2024
Revised: 16 November 2024
Accepted: 28 November 2024
Published: 6 December 2024

1. Introduction

Transportation fuels are the main artery of the transportation industry. The vital bulk chemicals, benzene, toluene, and xylenes (BTX), ensuring the high performance of fuels are usually found in a higher proportion in fossil fuels. Nevertheless, the production of these aromatics from fossil resources in using an energy-intensive process has a detrimental environmental impact. This is why developing eco-friendly alternatives to the latter process has become a priority. Using biomass as a feedstock and employing the catalysts in a process like catalytic pyrolysis can be an effective approach for producing a high-performance fuel by deoxygenating the resulting oil.

Jerzak et al. (2024) [1] provided a comprehensive review of biomass pyrolysis reactors, emphasising their adaptability to specific operational conditions and desired product yields. Fluidised bed reactors, including bubbling fluidised bed (BFB), circulating fluidised bed (CFB), and conical spouted bed (CSB), have been highlighted for their high efficiency in fast pyrolysis and significant bio-oil production. Gravity reactors, which utilise particle

free fall, are well suited for rapid or intermediate pyrolysis applications. Stationary-bed reactors, such as batch, semi-batch, and fixed-bed systems, stand out for their simplicity and flexibility, making them particularly suitable for laboratory-scale investigations. Mechanical reactors, including rotating cone, screw, and ablative pyrolysis systems, facilitate efficient mixing, continuous feed transport, and uniform heating, supporting diverse pyrolysis processes.

These reactor technologies enable the optimisation of pyrolysis based on biomass properties and target product specifications. Notably, many of these reactors are also employed for pyrolysis and the catalytic upgrading of pyrolysis oils. Two promising approaches have been distinguished for catalytic treatment based on the location of the catalytic process [2,3]. The first, which has been widely documented in the scientific literature, involves in situ catalytic treatment, where catalysts are directly integrated within the pyrolysis reactor. This method is particularly appreciated for its ease of implementation at the laboratory scale [4,5]. It allows for simultaneous pyrolysis and catalytic treatment in the same reactor, which has the advantage of reducing the number of required equipment and simplifying preparation and processing operations [6]. However, this in situ approach has certain limitations. Char, especially when rich in minerals, can form agglomerates over time that may incorporate catalyst particles, leading to their deactivation. Additionally, mixing the catalyst with biomass, char, and, possibly, the bed (which is often composed of sand in fluidised bed reactors) can result in a dilution of the catalyst within the reactor. The second approach, known as ex situ, involves catalytic treatment performed outside the pyrolysis reactor [7,8]. This method has the advantage of avoiding a mixture of the catalyst with the biomass and char in the reactor. It also allows for better control of temperature and residence time of the vapours in the catalytic bed [9]. In case of catalyst deactivation, the system can be regenerated using a method similar to that employed in Fluid Catalytic Cracking (FCC) reactors.

Xu et al. (2024) [10] investigated the use of thermal decomposition products from used lithium-ion batteries (PyNCM) as catalysts for the ex situ reforming of biomass pyrolysis volatiles, specifically from wheat straw. Their findings revealed that nickel and cobalt, recycled from battery cathodes, form over 35% of the catalyst and exhibit significant catalytic activity, increasing syngas production by 57.5% at 550 °C. Furthermore, the catalytic action of nickel, cobalt, and their oxides led to a 31.7% reduction in the oxygenated species in the bio-oil, enhancing deoxygenation. The optimal reforming temperature of 650 °C resulted in a maximum hydrogen yield of 2.66 mmol g^{-1}. This research underscores the potential of using thermal decomposition products from lithium-ion batteries as efficient catalysts for improving the syngas and bio-oil quality in biomass pyrolysis. However, their system was based on small biomass quantities, and the study did not address the catalyst behaviour or the evolution of products over time.

Liu et al. [11] conducted a noteworthy study on the in situ upgrading of Shengli lignite pyrolysis vapours using different metal-loaded HZSM-5 catalysts in a drop tube reactor (DTR) with pyrolysis temperatures ranging from 500 to 700 °C. Their study found that catalytic fast pyrolysis over metal-loaded HZSM-5 under mild conditions (an optimal temperature of 600 °C) could directly produce aromatics from solid lignite. The bifunctional metal-loaded HZSM-5 catalysts showed comparable catalytic activity for deoxygenation, leading to a decrease in oxygen content. The introduction of metal resulted in an increase in aromatics and a decrease in the organic oxygen species in the upgraded bio-oil. Among the catalysts, Ni-HZSM-5 exhibited the best performance in producing high-quality bio-oils with the highest aromatics content. The reactor used in their study has been previously reported [12]. The pyrolysis of biomass using fresh and regenerated HZSM5 catalysts after in situ deactivation was studied by Promsampao et al. [13].

At present, several catalysts have shown some activity and efficiency in the deoxygenation of bio-oil [2,14]. However, all of these catalysts remain very sensitive to deactivation, which is considered a handicap for industrial-scale installations [15,16]. Carbon deposition has emerged as a pervasive issue and the primary pathway for catalyst deactivation [17,18].

Carbon primarily originates from the polymerisation and polycondensation reactions that take place on the catalytic surface, leading to the creation of polyaromatic species. As a consequence, the active sites on the catalysts become obstructed [19].

This study represents a change in the reactor technology from our previous studies [20–22]. It firstly aims at studying the effect of a continuous DTR setup on the catalytic pyrolytic products and, also, attempts to monitor the stability of the catalyst by analysing the evolution of the composition of the liquid and gaseous products formed with operating time. By separating the pyrolysis process from the catalytic treatment, fine particles (char) blocking the pores of the catalyst is avoided, which allows for a longer reaction time to be able to properly follow the stability of the catalyst. Moreover, by varying the temperature of the catalytic reactor without changing that of the pyrolysis reactor, the temperature effect of the catalyst bed on the final products can also be investigated. To the best of our knowledge, limited research has been conducted on catalytic deoxygenation within a dual-stage reactor (DTR) system coupled with a catalytic fixed-bed to monitor the deoxygenation process over time using zeolite catalysts. This study aims to provide a comprehensive evaluation of the performance of such an integrated setup for biomass pyrolysis combined with catalytic deoxygenation.

2. Materials and Methods

2.1. Materials Used

This study used beech wood, which was obtained from ETS Lignex Company (Patornay, France) with an average particle size of 400 µm. The elemental and proximate analyses for the biomass are shown in Tables 1 and 2, respectively.

Table 1. Ultimate analysis of the biomass.

Biomass Used	Elemental Analysis (wt. %)			
	Carbon	Hydrogen	Nitrogen	Oxygen
Beech wood (BW)	47.38	6.11	<0.01	46.51

Table 2. Proximate analysis of the biomass based on TGA experiments (wt. %).

Biomass Used	Moisture Content	Volatile Matter	Fixed Carbon	Ash
Beech wood (BW)	5.70	75.93	17.52	0.85

2.2. HZSM-5 Catalyst Preparation

The catalyst employed in this study was a hydrophobic HZSM-5 zeolite in its protonated form (H^+), and it was supplied by ACS Materials in pellet form. These pellets were ground and sieved to obtain particles with sizes ranging from 1.0 to 1.4 mm. The apparent porosity of the catalyst was between 0.60 and 0.62. Prior to use, the catalyst underwent a calcination treatment in a tubular furnace. This process was conducted at atmospheric pressure, with a gradual temperature increase of 2 °C/min until reaching 550 °C. The catalyst was maintained at this temperature for 4 h in accordance with the protocol established in previous works [20–26].

2.3. Experimental and Analytical Setup

2.3.1. Experimental Setup

The experimental runs were performed in a continuous drop tube reactor coupled with a catalytic fixed-bed reactor, as illustrated by Figure 1. The use of such a configuration has been proven to enhance liquid yield [25], which was the main focus of this study. The two zones (pyrolysis and catalysis) were also independently controlled. This meant that the pyrolysis reaction could occur at a different temperature from the deoxygenation reaction. This kind of setup also enables following the catalytic de-activation and coke formation that only occur because of pyrolytic vapours.

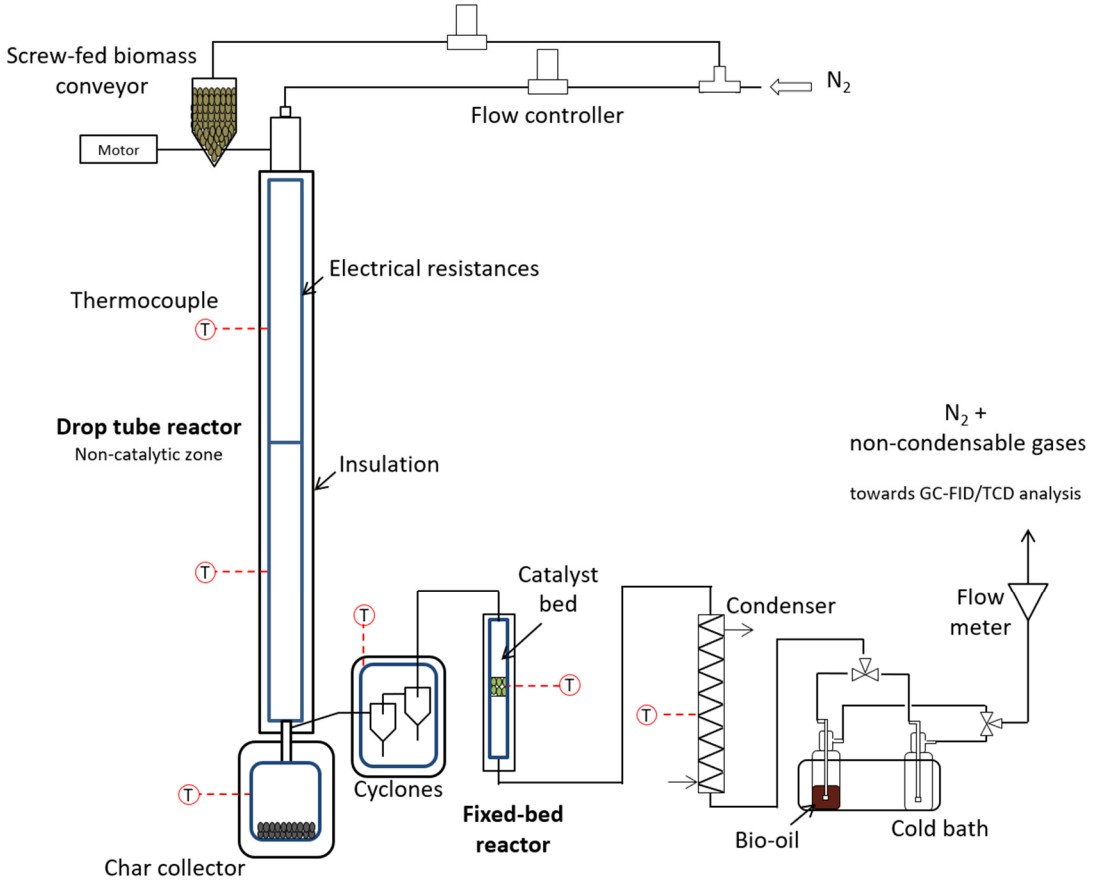

Figure 1. Global scheme of the drop tube reactor (DTR) system.

A screw conveyor (GLD 77.0, Tremie 5L from Gericke, Regensdorf, Switzerland) was used to feed biomass into the reactor through the top of the DTR. The heated length of the pyrolysis zone was 2 m high, and it possessed a 56 mm diameter. A char collector was placed at the bottom of the DTR to gather the solid residues from the biomass pyrolysis. It was heated to a temperature of 300 °C by a heating shell to ensure that the pyrolytic vapours penetrating it did not condense. However, some of the fine char particles tended to become entrained by the gas/vapour flow and escape the char collector. In order to separate these particles from the gaseous flux, two cyclones (efficiency: 85% each) were placed at the vapour exit of the DTR. The design of the cyclones was performed by the Cyclone 2.0 software considering the nitrogen flow rate and the flow rate of solid particles recovered at the reactor outlet. A stainless-steel fixed-bed reactor with an internal diameter of 13 mm was located at the exit of the second cyclone. A bed of catalyst was then placed inside the reactor. It should be noted that the whole system (except the catalytic fixed-bed reactor and the DTR, which were regulated independently) was kept at a temperature of 300 °C to prevent the condensation of the pyrolysis vapours.

For the experiments without any catalyst use, the pyrolysis experiments were performed by varying the DTR temperature (500, 550, and 600 °C) and the nitrogen flow rate (0.5, 1 and 2 L/min) at ambient conditions. For each experiment, the DTR was fed with 2 g/min of biomass. The DTR was set to the desired temperature, the nitrogen flow was measured at the exit to ensure no leakages, and the setup was then left to stabilise for two hours. After this period, the biomass was fed, and the reaction was allowed to take place for 120 min. After the experiment, the heating system was turned off and, then, the setup was allowed to cool to room temperature. After cooling, the oil was retrieved through the use of 99.98% pure acetone, which included a controlled quantity of nonane that was added as an internal addition in order to estimate the correct amount of acetone volatilised.

Concerning the experiments involving the presence of a catalyst, a 2 cm-high bed (1.48 g) of catalyst was placed in the fixed-bed reactor. The catalyst bed was held in place by thin layers of quartz wool placed at its top and bottom. The same experimental procedure as described above was used for these experiments. The only difference was that the bio-oil was collected, and the non-condensable gases were analysed at 10 min intervals to monitor any variation in their composition with time.

2.3.2. Analytical Setup for Pyrolytic Products

Afterwards, the protocol specified by Mohabeer et al. [21] was used to recover and analyse the resulting liquid and gaseous products. The bio-oil obtained was subjected to analysis using a GC-MS instrument (Varian 3900-Saturn 2100T from Agilent Technologies, Santa Clara, CA, USA) with a VF-1701ms (Agilent) column that had film thickness dimensions of 60 m × 0.25 mm × 0.25 µm. The temperature programme employed was identical to that of Charon et al. [27].

The identified constituents were compared to the mass spectra from the NIST library using Varian WS (WorkStation) and NIST 2002 software. Once the peaks were identified, their quantities were determined using a flame ionisation detector (FID) on a GC-FID Scion 456-GC Bruker instrument. The same column was used for the GC-MS analysis with the same temperature programme and a final temperature of 240 °C. These constituents were classified into "families" of chemicals based on their primary functional group.

CO, CO_2, CH_4, and H_2 were the primary constituents of the non-condensable gases (NCG). C_2H_2, C_2H_4, and C_2H_6 (represented as 'C_2') and C_3H_4, C_3H_6, and C_3H_8 (represented as 'C_3') were also present in minor proportions. A Perkin Elmer Clarus 580 gas chromatograph instrument was utilised to analyse the gases, which was equipped with both a flame ionisation detector (FID) and a thermal conductivity detector (TCD). The instrument included a Shincarbon St 100 120 column, a methaniser, and a hydrogen generator. Additionally, principal component analysis (PCA) was conducted.

PCA is a mathematical transformation technique that reduces the number of original dimensions to a new coordinate system with fewer dimensions [28]. This allows the data to be represented on a single graph, making it easier to interpret. The resulted score and loading plots depicted the samples and variables, respectively. In this case, the chemical groups recognised in the pyrolytic oils were considered as variables, whereas the samples were the diverse bio-oils obtained from the various experiments. For a more in-depth explanation and application of PCA to multivariate data, please refer to [28].

3. Results

3.1. Catalyst Characterisation Results

The specific surface of the HZSM-5 catalyst area was 285.7 m^2/g, and it had a pore size of approximately 5 Å, with a specific pore volume of 0.41 cm^3/g. To prepare the catalyst for use, it was ground and sieved to a size range of 1.2 to 1.0 mm, and it had an apparent porosity of 0.61. Before use, the catalyst was calcined at atmospheric air pressure at a heating rate of 2 °C/min, reaching 550 °C and holding for 4 h.

For the FT-IR acidity analysis, infrared spectroscopy stood out as the most effective method for investigating zeolite acidity. The zeolites demonstrated two distinct forms of acidity. The first type involved the hydroxyl groups that bridge the Si and Al atoms in the H-form of zeolites, which are considered potent Brønsted acid sites. The second type comprises Lewis acid sites, which are typically linked to the aluminium and oxygen species located outside the zeolite framework. For the acidity characterisation, after pyridine adsorption, the stepwise desorption of the catalysts used was performed at 150 °C. Figure 2 presents the stepwise desorption FTIR spectra for the HZSM-5 catalyst found in the range considered. The HZSM-5 spectrum exhibits characteristic bands at 1594 and 1580 cm^{-1}, which are indicative of Brønsted acid sites, while the bands at 1486 and 1436 cm^{-1} represent Lewis acid sites.

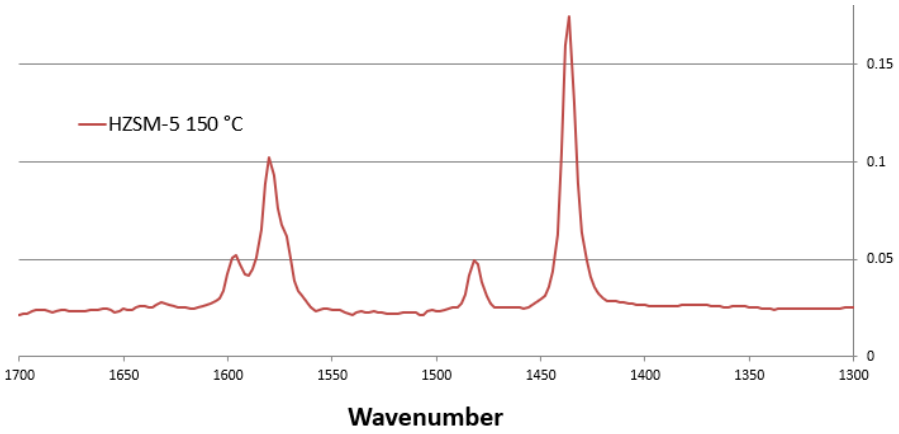

Figure 2. The FT-IR spectra for HZSM-5 between 1700 and 1300 cm^{-1} at 150 °C.

To examine the crystalline structure, X-ray diffraction (XRD) analysis was employed. Figure 3 illustrates the resulting diffraction patterns. The catalyst displayed diffraction peaks characteristic of the HZSM-5 zeolite structure. The XRD analysis showed the superposition of the peaks from both the fresh and used catalyst, indicating that the structure of the catalyst had not been impacted by the reaction.

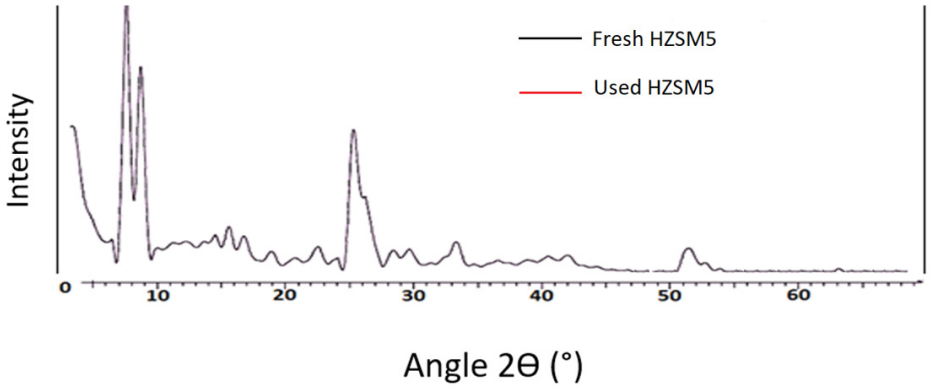

Figure 3. XRD profiles of the fresh and spent catalysts.

3.2. Defining Optimal Conditions for Pyrolysis Reaction

The pyrolysis of beech wood in the *DTR* was investigated at three distinct reaction temperatures (500, 550, and 600 °C) and also three pyrolysis vapours gas residence time (using 0.5, 1, and 2 L/min N_2 as carrier gas), which were calculated as follows:

$$\tau_p = \frac{V_{DTR}}{Q_{v\ N2}}.$$

In this case, the whole setup downstream of the *DTR* was maintained at 300 °C. The different experiments conducted have been listed in Table 3. It should be noted that the gas residence time was calculated based on the nitrogen flow rate.

The molecules detected by GC-MS were represented in the chemical families, as shown in Table 4. The detailed composition of the oil is given in Appendix A.1 (Table A1).

Figure 4 demonstrates the different values obtained for the mass balances of the various experimental runs. The yields shown in Figure 4 were indeed on a dry basis. It should be noted that values of more than 85% were experimentally found. The gap in the values can be explained by the fact that, despite all the efforts to recover all of the liquid produced, there was still a fraction that remained on the walls of the DTR installation, which was lost. Hence, the mass balances were completed to 100% with respect to the liquid fraction.

Table 3. The pyrolysis experiments without catalyst use.

DTR Temperature (°C)	Nitrogen Flow Rate (mL/min) *	Gas Residence Time (min)
500	500	9.27
	1000	4.63
	2000	2.32
550	500	9.27
	1000	4.63
	2000	2.32
600	500	9.27
	1000	4.63
	2000	2.32

* At room temperature and atmospheric pressure.

Table 4. The major chemical groups detected in bio-oil by GC-MS.

Retention Time (min)	Reference Compound for Calibration	Chemical Group	Most Abundant Compound in Oil	
6.38	Furan	Furans	Furan, 2,3,5-trimethyl-	$C_7H_{10}O$
10.90	Acetic acid	Carboxylic acids	Acetic acid	$C_2H_4O_2$
18.14	Allyl butyrate	Esters	2-Propanol, 1,1-dimethoxy-, acetate	$C_7H_{14}O_4$
21.40	2-Cyclopenten-1-one, 2-methyl	Ketones	Levoglucosenone	$C_6H_6O_3$
28.02	Furfural	Aldehydes	Furfural	$C_5H_4O_2$
28.66	Phenol	Phenols	Phenol, 2,4,5-trimethyl-	$C_9H_{12}O$
30.43	Dodecene	Alkenes	Cyclopentene, 1-(1-methylethyl)-	C_8H_{14}
34.88	p-Cresol	Alcohols	2-Furanmethanol	$C_5H_6O_2$
39.29	Tetradecane	Alkanes	Nonane, 4-ethyl-5-methyl-	$C_{12}H_{26}$
41.72	4-Methylcatechol	Guaiacols	4-Ethyl guaiacol	$C_9H_{12}O_2$
42.66	Benzamide	Amides	Butyramide, 2,2,3,3-tetramethyl-	$C_8H_{17}NO$
49.49	Levoglucosan	Sugars	Levoglucosan	$C_6H_{10}O_5$

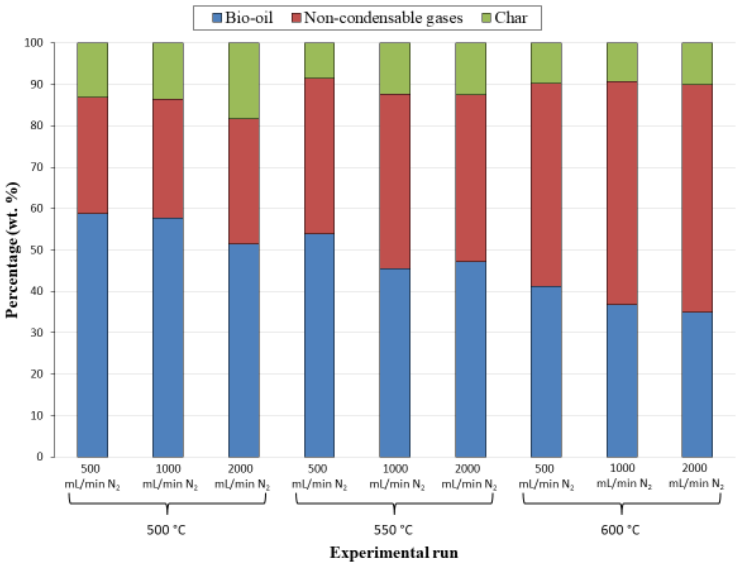

Figure 4. Mass balances of the experiments performed without catalyst use.

What can be observed from Figure 4 is that, firstly, the lowest temperature (500 °C) corresponded to the highest amount of char produced (between 13 and 18 wt.%) and the lowest amount of non-condensable gases formed (between 28 to 30 wt.%). In contrast to the former observations, 600 °C, the highest temperature tested, produced the lowest amount of char (around 9 to 10 wt. %) and the highest amount of non-condensable gases (49–55 wt.%). It was also noted that the experiment at 500 °C under 500 mL/min N_2 yielded the highest amount of bio-oil (58.8 wt.%). As observed, the highest amount of

bio-oil production (58.8 wt.%) was obtained from the experiment conducted with a nitrogen flow rate of 500 mL/min at a temperature of 500 °C. Indeed, the reactions that had a shorter gas residence time were not able to generate more oil. Further calculations were made to understand this phenomenon. In addition, it was seen that the biomass particle residence time in the reactor was 2.20 s, which is much lower than the gas residence time indicated in Table 3. This observation means that the limiting parameter, that is, the parameter that controlled the formation of the products and dynamics of the reaction is the biomass particle residence time and not the gas residence time. This points to the fact that even if the carrier gas flow rate were increased, hence reducing gas residence time, no significant change would be brought to the liquid product distribution as long as the pyrolysis reaction takes place in the same pyrolysis regime, that is, where the biomass particle residence time is shorter than the gas residence time. This observation has also been verified by Guizani et al. [29], Jahirul et al. [30], and Ellens [31]. As a result, the following operating conditions were adopted for the experiments whole series involving the catalyst use undertaken in this part of the study: 500 °C under 500 mL/min N_2.

3.3. Effect of HZSM-5 Catalyst Use on Pyrolytic Product Distribution

A catalyst mass of 1.48 g, corresponding to a catalyst bed volume of 2.70 mL, was used for all the experiments. The catalyst's apparent porosity was 0.61. The contact time was estimated to be 0.20 s between the gas and the catalyst bed. The temperature of the fixed-bed reactor was varied (425, 450, and 500 °C) so as to study the effect on the pyrolytic products. The DTR temperature and the carrier gas flow rate were fixed at 500 °C and 500 mL/min, as mentioned earlier.

It has already been shown that the presence of a catalyst-boosted non condensable gases NCG formation inhibits the liquid formation as the deoxygenation process takes place [21]. Figure 5 confirms these findings, although a different experimental setup was used (a percentage error of ~1% was found for the DTR). The product distributions illustrated in Figure 5 are those recovered from t = 0 min until the end of the reaction. It can also be noticed that, even at a temperature of 425 °C, a catalytic effect was observed.

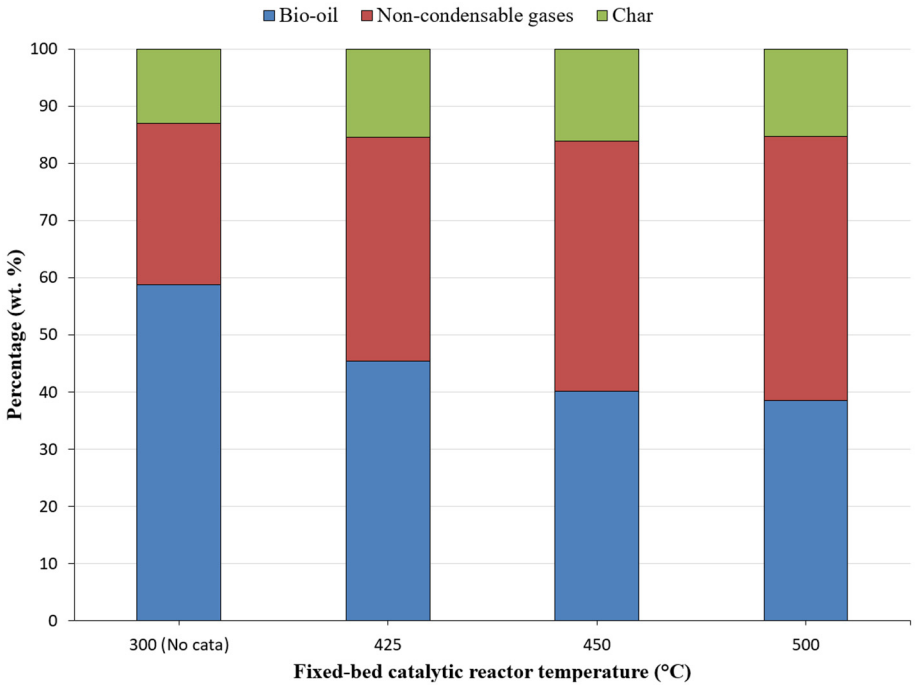

Figure 5. The catalytic effect on the pyrolytic product distribution.

3.4. Effect of Varying the Fixed-Bed Reactor Temperature on the Catalytic Pyrolytic Liquid and Gas Products

In the catalytic fixed-bed reactor, the deoxygenation reaction continually takes place. The main aims of the experiments to be presented is to investigate the catalytic performance in the continuous regime, the effect of the bed temperature on the products formed, and the stability of the catalyst in time during the reaction. In the literature, it has been observed that the catalyst, after one hour of use, starts losing some of its activity and starts to de-activate [23–26]. This de-activation usually affects the pyrolytic product distribution [21].

3.4.1. Analysis of the Carboxylic Acid Evolution with Rising Catalytic Fixed-Bed Reactor Temperature

Carboxylic acids are the major family of untreated pyrolytic oil, as stated in the literature [20]. It is thus interesting to follow their evolution over the time in order to monitor the catalyst's performance. This evolution was followed for the molar percentage of the acids and, also, the calculated mass flow rate (g/min) corresponding to these percentages. Figure 6 depicts the percentage (mol.%) of the carboxylic acids, as obtained in the bio-oils collected at different catalytic fixed-bed reactor temperatures along with their mass flow rate at t = 10 min for different catalytic fixed-bed reactor temperatures.

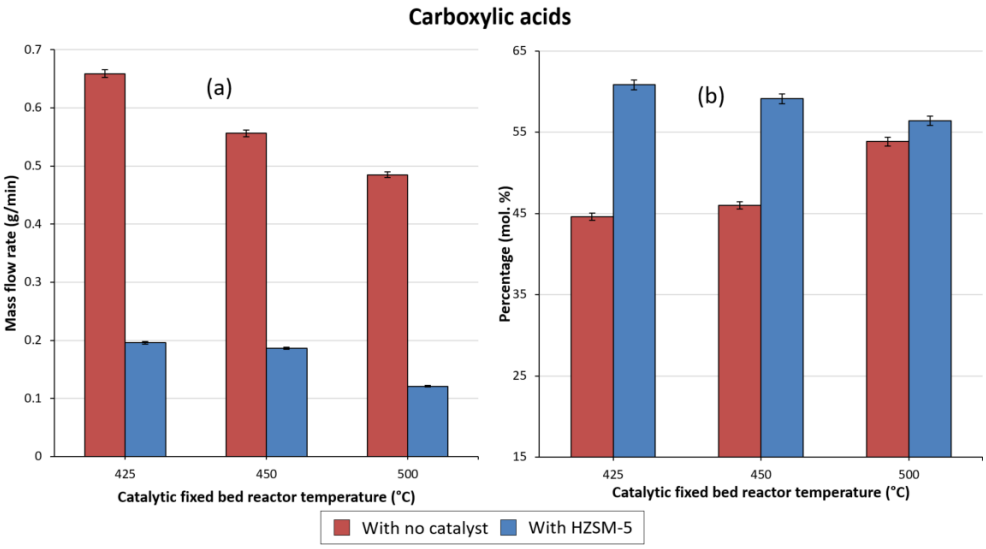

Figure 6. Evolution of (**a**) the mass flow rate (g/min) and (**b**) percentage (mol.%) of carboxylic acids at t = 10 min at different catalytic fixed-bed reactor temperatures.

Several observations can be made from Figure 6. Firstly, some similarities were found in the evolution trend in mass flow rates and percentages for the experiments performed while using HZSM-5; both series showed a decrease in carboxylic acids as the catalytic fixed-bed reactor temperature increased. This is in line with what can be seen in Figure 5. Indeed, with increased catalytic reactor temperature, less liquid was recovered. Hence, it can be said that increasing the catalytic reactor temperature boosted the catalytic activity, enhancing the different deoxygenation reactions, including decarboxylation, which resulted in a lower amount of carboxylic acids being present in the collected bio-oil. However, one main difference was found concerning the experiments conducted without the use of catalysts: the mass flow rates showed a decrease with an increase in the reactor temperature, while the percentages demonstrated an increase. The decreasing trend appeared to be more coherent as it showed that the chemical group was converted through the homogeneous cracking reaction occurring without the use of catalysts. Several articles in the literature base their results on the percentage of chemical families that are present in bio-oils [32–35]; this method of comparison may give rise to misleading conclusions if other, deeper analyses are not conducted.

Now, as mentioned earlier, in order to better comprehend the impact of catalyst use on the liquid product, bio-oil samples were recovered intermittently and analysed to obtain an idea of their composition. Then, conversion and production rates, as previously explained [21] (details are provided in the Appendix A.2), were calculated for each chemical family found in the oils. Table 5 details the values obtained for the bio-oil recovered at a catalytic fixed-bed reactor temperature of 500 °C. Those obtained for the 450 and 425 °C temperatures are listed in the Appendix A.1 (in Tables A2 and A3). The rates obtained from t = 0 to t = 35 min were omitted from the table as the reaction had not reached the steady state yet.

Table 5. The conversion and production rates of the chemical families present in the upgraded bio-oils at a catalytic fixed-bed reactor temperature of 500 °C.

Chemical Families	Conversion ("−" Sign) and Production ("+" Sign) Rate (%)		
	t = 35 min	t = 60 min	t = 120 min
Carboxylic acids	−69	−69	−49
Alkanes	−68	−74	−55
Aromatics	−81	−83	−77
Alcohols	−75	−77	−61
Aldehydes	−53	−54	−22
Amides	−71	−71	−25
Ketones	−66	−67	−49
Esters	−49	−52	−61
Furans	−8	−19	−2
Guaiacols	−55	−50	−2
Phenols	−71	−76	−59
Carbohydrates	−87	−87	−89

Several deductions can be made following these tables. Initially, it appeared that, for all temperatures, the trend was the same: the conversion rate for almost all families became less important over time. This is proof that the catalyst loss indeed gradually occurred in its activity during the reaction and, so, become less efficient. However, another difference that was noticed was the fact that, according to the fixed-bed reactor temperature, the efficiency of the catalyst experienced a change. As can be seen from comparing the values for all temperatures, the higher the fixed-bed reactor temperature was, the more performant was the catalyst in converting the chemical families. For instance, if carboxylic acids were considered, the deoxygenation at 500 °C ensured a first conversion at −69%; another first conversion occurred at −69% at 450 °C; and, lastly, one at −49% at 425 °C. It can hence be stipulated that the deoxygenation at 500 °C was more successful.

3.4.2. Principal Component Analysis (PCA) of the Pyrolytic Oils Obtained at Different Catalytic Fixed-Bed Reactor Temperatures

Another technique that was employed to study the correlations and differences between the bio-oil content at 500 mL/min N_2 at different pyrolysis temperatures was the PCA. The results are illustrated in Figure 7. The variability observed in the bio-oils produced at different pyrolytic temperatures was described by the first two principal components (F1 and F2), which accounted for 39.56% and 21.99% of the variability, respectively. It is important to note that the analytical setup had an accuracy of 1%, and the concentrations below 1% were disregarded to ensure an accurate representation of the data spread. By comparing the two plots in Figure 7a,b, it was possible to identify the various co-variations between the oils and the different groups present in them.

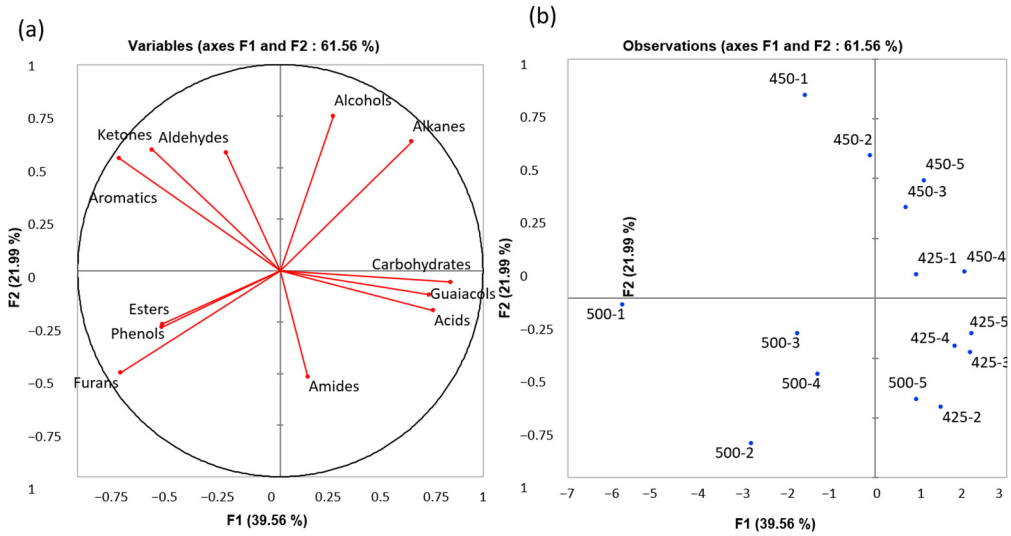

Figure 7. PCA of the beech wood bio-oil samples in the DTR with HZSM-5 at different catalytic fixed-bed reactor temperatures, (**a**) Correlation circle, (**b**) Score plot.

For instance, the fact that, in Figure 7a, the experiments performed at 450 and 425 °C were gathered close together in a sub-group meant that they presented the same pyrolytic behaviour. Meanwhile, the samples collected for the experiment at 500 °C presented a distinct sub-group, exposing a different behaviour.

The loading plot in Figure 7a can be used to determine the variables that had the most significant impact on F1 and F2. These variables, referred to as "important variable" were found to be aromatics, phenols, and ketones. Typically, samples that are situated on the same side of the axes are positively correlated and vice versa. It can be witnessed that the carboxylic acids and phenols were negatively correlated along F1, hence meaning that when one of them was converted, the other one was produced. The latter statement can be witnessed in Table 5, where the conversion degree of the carboxylic acids decreased with the reaction time, while that of the phenols increased with reaction time.

3.4.3. Stability of the Catalyst During Continuous Pyrolysis Reaction

As mentioned earlier, when the catalyst had been in continual use during a continuous pyrolysis reaction for some time, it started to display a decrease in activity. Figure 8 represents the effect of the catalyst de-activation on the colour of the collected bio-oil in time during the catalytic pyrolysis of the biomass.

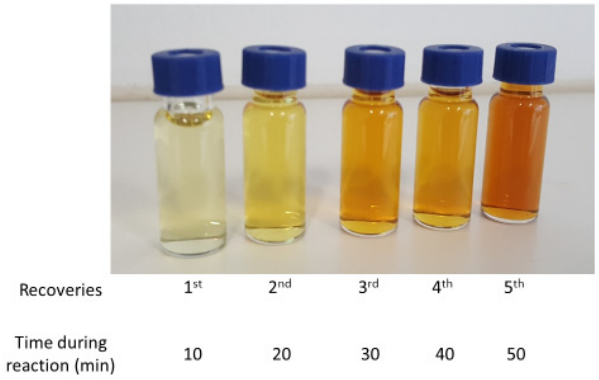

Figure 8. Effect of the catalyst de-activation on the bio-oil obtained during pyrolysis reaction.

Studying this de-activation and its impacts on product distribution is of utmost importance to fully comprehend the reaction in its entirety. For this, the chemical family mostly present in the bio-oil obtained without the use of the catalyst—and which most impacted

the behaviour of the bio-oil [20,36], that is, the carboxylic acids—was taken as a case in point. Figure 9 represents the evolution of the mass flow rate (g/min) of the carboxylic acids, phenols, and alcohols, respectively, during the catalytic pyrolysis reaction at different catalytic fixed-bed reactor temperatures. These three chemical groups formed part of the major ones present in the bio-oil [20]. Only the last three bio-oil recoveries are presented (t = 35, 60, and 120 min). Once again, the values obtained from t = 0 to t = 35 min were omitted from the table as the reaction had not reached the steady state yet.

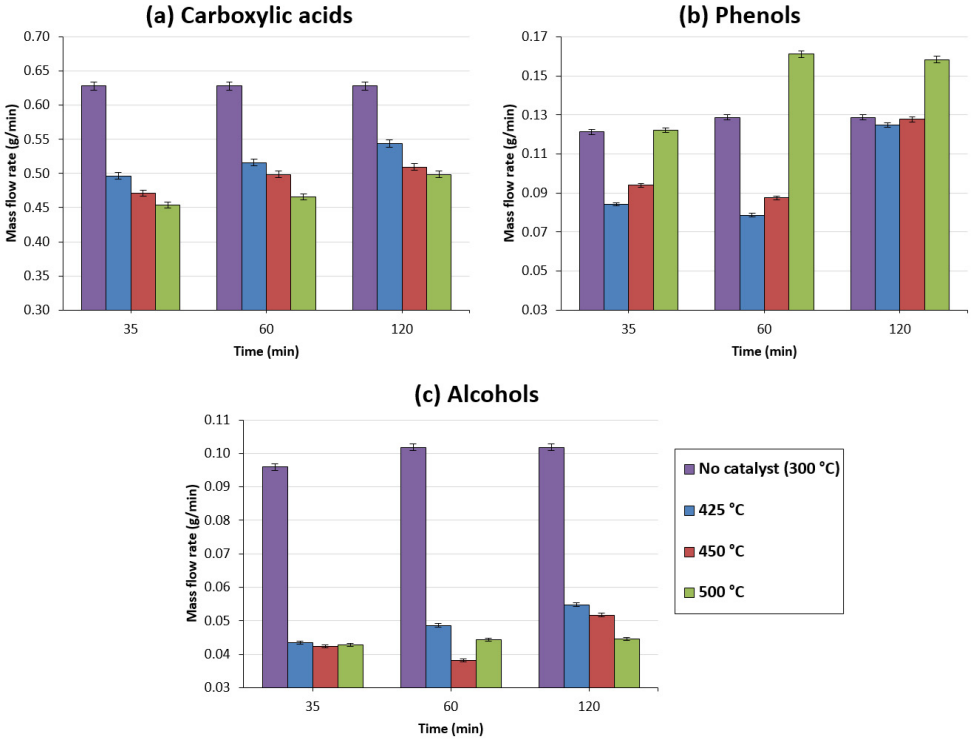

Figure 9. Evolution of the (**a**) carboxylic acids, (**b**) phenols, and (**c**) alcohols in the liquid product (g/min) in time with different catalytic fixed-bed reactor temperatures.

Initially, the same behaviour as discussed above was noted: the mass flow rate of the carboxylic acids demonstrated a steady decrease as the catalytic fixed-bed reactor temperature increased. Furthermore, as was observed, the mass flow rate of the carboxylic acids also showed a steady increase during the reaction at a given temperature for all catalytic fixed-bed temperatures (such as, for instance, at t = 35 min, 0.45 g/min vs. t = 120 min, and 0.50 g/min with no catalyst). However, the mass flow rates of the catalytic bio-oils remained less than those obtained for the non-catalytic bio-oil. This proved that, even at 425 °C, the catalyst did display a deoxygenation performance. Now, the increase in the mass flow of the carboxylic acids during the reaction was proof that the catalytic activity tended to decrease as the reaction continued in time. Additionally, for the phenols, an inverse trend, when compared to the carboxylic acids, was observed. Indeed, the mass flow rates of the phenols increased as the reaction proceeded, and they became more important as higher catalytic temperatures were used. It can be inferred that the conversion of carboxylic acids gives rise to the production of phenols; these two chemical families are very strongly negatively correlated [20]. Also, as observed in our previous studies [21], carboxylic acids are converted to aromatics and phenols under the action of HZSM-5 at 500 °C. The data presented in Table 5 further support this observation; the conversion rates of the carboxylic acids decreased with time, meaning that fewer acids were converted and those of aromatics and phenols followed, confirming that the latter families were generated from acids. Finally, for the alcohols, no definitive observation can be made. The mass flow rates at all catalytic temperatures were less than that obtained without the use of catalysts;

however, the catalytic temperature did not cause any significant conversion or production of this chemical group.

3.4.4. Gas Product Composition

The NCG samples were also recovered intermittently at the same times as the bio-oil sample recoveries, and the same kind of analyses that were conducted for the bio-oil samples was performed on them. Figure 10 depicts, compared to that which was obtained under the same experimental conditions without the use of any catalyst, the gas product distribution obtained for a sample at a fixed-bed reactor temperature of 500 °C under 500 mL/min with the use of HZSM-5.

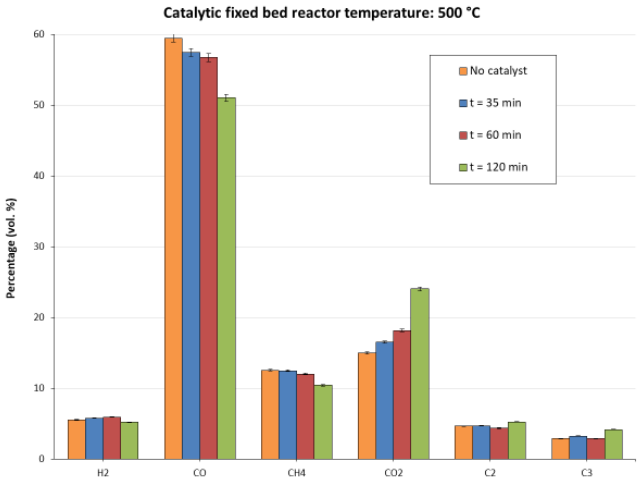

Figure 10. Evolution of the NCG composition (vol.%) in time at 500 °C (catalytic fixed-bed reactor vs. no catalyst).

It was first seen that the evolutions for the reactions at the fixed-bed reactor temperatures of 500, 450, and 425 °C followed the same trend. Here, the focus was on the one at 500 °C. As can be observed, the composition of the NCG did not undergo a drastic change during the analyses up to 60 min of reaction time compared to the reaction without a catalyst. A real change was noticed at t = 120 min, where the CO and CH_4 percentages dropped and the CO_2, C_2, and C_3 ones experienced an increase. As the percentages stood after two hours of reaction, it can be said that the decarboxylation reaction (production of CO_2) was privileged in time relative to the decarbonylation one (formation of CO). Also, according to Gayubo et al. [37], carboxylic acids undergo decarboxylation under the action of HZSM-5 to give rise to ketones as intermediates and alkenes as end products. Hence, the increase in C_2 and C_3 can be related to the deoxygenation of carboxylic acids.

However, the values obtained for the conversion and production rates for the NCG components did not reflect the same trend as that demonstrated for the chemical families in the liquid product. In the latter case, the conversion rate tended to decrease, showing a decreasing activity of the catalyst; here, no definite tendency was observed. Also, from t = 120 min onwards, severe clogging problems were experienced within the experimental installation. It was theorised that the coke formed on the surface of the catalyst bed and the solid particles deposited on the catalyst surface caused a severe pressure drop, which gave rise to a pressure build up inside the setup. It subsequently caused an important drop in the gas flow at the exit of the installation. This phenomenon repeatedly happened for every reaction.

4. Conclusions

This study presents the continuous pyrolysis of the biomass in a drop tube reactor (DTR) with the use of a catalyst. The aim was first to study the effect of this kind of setup on the pyrolytic products and also to attempt to periodically monitor the de-activation of

the catalyst by analysing the evolution of the composition of the liquid and the gaseous products formed. The DTR temperature and gas residence time were, primarily, varied to examine the pyrolytic products. It was found that the reaction parameters yielding the maximum bio-oil yield without the use of catalysts were as follows: 500 °C under 500 mL/min N_2 (~58 wt.%). A glance at the conversion and production rates of the chemical families present in the liquid product showed that HZSM-5 lost its deoxygenation efficiency steadily over time as the conversion rates of the families decreased. However, with the present setup, from t = 120 min onwards, severe clogging problems were repeatedly experienced within the experimental installation. A fluidised bed reactor, involving agitation of the bed instead of the installation chosen for this reactor, might present the best results for such a process.

Author Contributions: Conceptualisation, C.M., L.A., B.T. and Z.B.; methodology, C.M., L.A., B.T. and Z.B.; validation, C.M., B.T. and A.M.; formal analysis, C.M.; investigation, B.T.; resources, B.T.; data curation, B.T.; writing—original draft preparation, L.A.; writing—review and editing, C.M.; visualisation, C.M.; supervision, L.A.; project administration, L.A.; funding acquisition, B.T. All authors have read and agreed to the published version of the manuscript.

Funding: Funding for this project was provided by the European Union through the European Regional Development Fund (ERDF) and the Regional Council of Normandie, Agreement number: HN0002485.

Institutional Review Board Statement: Ethical review and approval were waived for this study as it did not require ethical approval.

Informed Consent Statement: Not applicable.

Data Availability Statement: The results are available upon request and can also be accessed in the PhD thesis of Mohabeer Chetna (available at the following link (3 December 2024): https://theses.fr/2018NORMIR22, accessed on 10 May 2024).

Conflicts of Interest: The authors declare no conflicts of interest and the funders had no role in the design of the study; in the collection, analyses, or interpretation of data; in the writing of the manuscript; or in the decision to publish the results.

Appendix A

Appendix A.1. Detailed Composition of the Bio-Oil in Different Cases

Table A1. Detailed composition of the bio-oil without catalyst at 500 °C, as determined by GC-FID.

Name	Conc. (mg/mL)	Formula
Propanoic acid, anhydride	0.05696848	$C_6H_{10}O_3$
1,2,3-Propanetriol, 1-acetate	0.157665431	$C_5H_{10}O_4$
Acetic acid, 1-methylethyl ester	1.1150756	$C_5H_{10}O_2$
2-Propanol, 1,1-dimethoxy-, acetate	0.022405046	$C_7H_{14}O_4$
Cyclobutene, 2-propenylidene	0.072427252	C_7H_8
2-Propanol	0.02001388	C_3H_8O
Propanoic acid	0.039777747	$C_3H_6O_2$
3-Penten-2-one, 4-methyl-	0.020135457	$C_3H_4O_2$
Cyclopentanone	0.029802766	C_5H_8O
Methane, isocyanato-	0.01918618	C_2H_3NO
1,2,3-Propanetriol, monoacetate	0.032753012	$C_5H_{10}O_4$
1,2,3-Propanetriol, diacetate	0.036080879	$C_7H_{12}O_5$
Butyramide, 2,2,3,3-tetramethyl-	0.22577449	$C_8H_{17}NO$
Butanoic acid, pentyl ester	0.05561872	$C_9H_{18}O_2$
3-Ethoxycarbonyl-5-hydroxytetrahydropyran-2-one	0.023443187	$C_8H_{12}O_5$
2-Hexanone, 4-hydroxy-5-methyl-	0.049436952	$C_7H_{14}O_2$
3-Cyclopentyl-1-propanol	0.01962652	$C_8H_{16}O$
2-Cyclopenten-1-one	0.031693789	C_5H_6O

Table A1. *Cont.*

Name	Conc. (mg/mL)	Formula
Furfural	0.03993002	$C_5H_4O_2$
2-Pentanone, 4-hydroxy-4-methyl-	0.024279481	$C_6H_{12}O_2$
Cyclobutanemethanol	0.02099842	$C_5H_{10}O$
2-Furanmethanol	0.040587	$C_5H_6O_2$
Propane-1,1-diol diacetate	0.020340311	$C_7H_{12}O_4$
2-Butynamide, N-methyl-	0.23169856	C_5H_7NO
1,4-Dioxane, 2-ethyl-5-methyl-	0.03172624	$C_7H_{14}O_2$
Acetylfuran	0.32278454	$C_6H_6O_2$
2-Cyclopenten-1-one, 2-hydroxy-	0.019380296	$C_5H_6O_2$
Levoglucosenone	0.05762254	$C_6H_6O_3$
1,1-Bicyclohexyl-1,1-diol	0.04907126	$C_{12}H_{22}O_2$
2-Cyclopenten-1-one, 2-hydroxy-3-methyl-	0.020890618	$C_6H_8O_2$
n-Butyric acid 2-ethylhexyl ester	0.026979851	$C_{12}H_{24}O_2$
2-Cyclopenten-1-one, 3,4-dimethyl-	0.028779242	$C_7H_{10}O$
2(5H)-Furanone	0.028754278	$C_4H_4O_2$
Cyclohexanone, 2-(hydroxymethyl)-	0.023979913	$C_7H_{12}O_2$
1,3-Cyclopentanedione, 2-methyl-	0.020297723	$C_6H_8O_2$
1-Hydroxymethyl-2-methyl-1-cyclohexene	0.019337908	$C_8H_{14}O$
2-Cyclopenten-1-one, 2,3,4-trimethyl-	0.018693786	$C_8H_{12}O$
2-Cyclopenten-1-one, 3-ethyl-2-hydroxy-	0.021421103	$C_7H_{10}O_2$
Phenol	0.1323347	C_6H_6O
2-Cyclopenten-1-one, 2,3-dimethyl-	0.01953008	$C_7H_{10}O$
2-Cyclopenten-1-one, 3-ethyl-2-hydroxy-	0.036549287	$C_7H_{10}O_2$
Maltol	0.01959962	$C_6H_6O_3$
Phenol, 2,5-dimethyl-	0.02755256	$C_8H_{10}O$
2,5-Furandicarboxaldehyde	0.021066138	$C_6H_4O_3$
Phenol, 2-methyl-	0.05927378	C_7H_8O
Phenol, 3-ethyl-5-methyl-	0.0998888	$C_9H_{12}O$
Cinnamaldehyde, beta-methyl-	0.02060191	$C_{10}H_{10}O$
4,7-Methano-1H-indene-1,8-dione, 3a,4,7,7a-tetrahydro-	0.022425904	$C_{10}H_8O_2$
Phenol, 3,5-dimethyl-	0.02751962	$C_8H_{10}O$
2-Ethyl-2-hydroxy-1,3-dimethylcyclopentanecarboxylic acid, ethyl ester	0.052890251	$C_{12}H_{22}O_3$
Phenol, 2,4,6-trimethyl-	0.03430526	$C_9H_{12}O$
Phenol, 2,4-dimethyl-	0.02475266	$C_8H_{10}O$
Phenol, 4-ethyl-	0.03064892	$C_8H_{10}O$
Phenol, 2-ethyl-	0.02794784	$C_8H_{10}O$
Phenol, 3,4,5-trimethyl-	0.06945224	$C_9H_{12}O$
2,3-Anhydro-d-galactosan	0.0543331	$C_6H_8O_4$
Phenol, 2,3,5-trimethyl-	0.02518088	$C_9H_{12}O$
Phenol, 2,3,5-trimethyl-	0.0494906	$C_9H_{12}O$
Phenol, 2-methyl-5-(1-methylethyl)-	0.03048422	$C_{10}H_{14}O$
1H-Inden-1-one, 2,3-dihydro-2-methyl-	0.019236753	$C_{10}H_{10}O$
2-(1-Cyclopentenyl)furan	0.32740209	$C_9H_{10}O$
Resorcinol (1,3-Benzenediol)	0.02078322	$C_6H_6O_2$
Benzene, 1-methoxy-4-(1-methylpropyl)-	0.13543352	$C_{11}H_{16}O$
Benzene, 3-ethyl-1,2,4,5-tetramethyl-	0.016637476	$C_{12}H_{18}$
2-Methyl-5-hydroxybenzofuran	0.36329039	$C_9H_8O_2$
2-Allyl-4-methylphenol	0.0279149	$C_{10}H_{12}O$
1,2-Benzenediol, 4-methyl-	0.04285198	$C_7H_8O_2$
2,5-Dimethylhydroquinone	0.020235313	$C_8H_{10}O_2$
1,2-Diethoxy-4-ethylbenzene	0.023552716	$C_{12}H_{18}O_2$
1,4-Benzenediol, 2,6-dimethyl-	0.02052498	$C_8H_{10}O_2$
1,5-Dihydroxy-1,2,3,4-tetrahydronaphthalene	0.015180556	$C_{10}H_{12}O_2$
1,3-Benzenediol, 4-ethyl-	0.01908852	$C_8H_{10}O_2$
2(3H)-Naphthalenone, 4,4a,5,6,7,8-hexahydro-1-methoxy-	0.020672183	$C_{11}H_{16}O_2$
3-Penten-2-one,4-(6,7,7-trimethyl-2,3-dioxabicyclo [2.2.2]oct-5-en-tyl)	0.019686105	$C_{14}H_{20}O_3$
2,5-Dimethoxyphenethylamine	0.22472554	$C_{10}H_{15}NO_2$
Levoglucosan	0.21422338	$C_6H_{10}O_5$

Appendix A.2. Conversion and Production Rate

The following tables (Tables A2 and A3) list the conversion (−) and production (+) rates of the different chemical families obtained in the presence of a catalyst in time. The calculation used to obtain these values is the following:

$$x_A = \left(\frac{x_{A_0} - x_{A_1}}{x_{A_0}} \right) \times 100\%,$$

where x_A is the conversion rate of Family A;

x_{A_0} is the no. of moles of A obtained without de-oxygenation;

x_{A_1} is the no. of moles of A obtained after de-oxygenation.

It should be noted that a negative sign in front of a value indicates a reduction, and a positive sign indicates an increase or a production. The "production" marking means that the chemical family, or non-condensable gas component, was produced because of the catalytic treatment when it was not present in the original, non-catalytic, product. Another important point is that the conversion rates presented do not take into account the water content of the bio-oil, which was already subtracted from the beginning of the calculations.

Table A2. Conversion and production rates of the chemical families present in the upgraded bio-oils at 450 °C.

Chemical Families	Conversion ("−" Sign) and Production ("+" Sign) Rate (%)				
	t = 10 min	t = 20 min	t = 35 min	t = 60 min	t = 120 min
Carboxylic acids	−88	−79	−63	−51	−12
Alkanes	−74	−56	−25	+6	+219
Aromatics	−92	−89	−82	−82	−48
Alcohols	−92	−89	−83	−81	−52
Aldehydes	−84	−78	−63	−49	+9
Amides	−91	−90	−86	−86	−54
Ketones	−84	−77	−66	−73	−27
Esters	−93	−89	−81	−61	−22
Furans	−85	−76	−58	−63	−5
Guaiacols	−87	−80	−60	−47	+48
Phenols	−91	−90	−83	−81	−43
Carbohydrates	−98	−97	−91	−87	−59

Table A3. Conversion and production rates of the chemical families present in the upgraded bio-oils at 425 °C.

Chemical Families	Conversion ("−" Sign) and Production ("+" Sign) Rate (%)				
	t = 10 min	t = 20 min	t = 35 min	t = 60 min	t = 120 min
Carboxylic acids	−85	−53	−43	−35	−23
Alkanes	−85	−55	−50	−26	−33
Aromatics	−92	−78	−76	−67	−65
Alcohols	−92	−82	−76	−70	−62
Aldehydes	−91	−70	−61	−45	−36
Amides	−92	−46	−65	−17	−45
Ketones	−89	−69	−64	−42	−37

Table A3. *Cont.*

Chemical Families	Conversion ("−" Sign) and Production ("+" Sign) Rate (%)				
	t = 10 min	t = 20 min	t = 35 min	t = 60 min	t = 120 min
Esters	−92	−78	−74	−43	−43
Furans	−75	−15	−16	−32	−31
Guaiacols	−87	−52	−36	+3	+50
Phenols	−94	−76	−73	−65	−50
Carbohydrates	−99	−93	−89	−80	−76

Appendix A.3. The Evolution of the Composition of Chemical Families in Time (vol.%)

The evolution in time (vol.%) of the chemical families' composition is illustrated in Table A4.

Table A4. The bio-oil compositions (mol.%) obtained during reaction at different catalytic fixed-bed reactor temperatures with and without HZSM-5.

		Bio-Oil Composition (mol. %)														
Fixed-Bed Reactor Temperature	**No Catalyst**	**425 °C**					**450 °C**					**500 °C**				
Time in Reaction (min)	**-**	**10**	**20**	**35**	**60**	**120**	**10**	**20**	**35**	**60**	**120**	**10**	**20**	**35**	**60**	**120**
Carboxylic acids	47.44	60.83	61.11	61.66	55.01	55.28	50.57	56.94	59.11	62.56	53.30	48.10	54.73	52.37	53.45	58.25
Alkanes	0.36	1.47	1.42	1.34	1.55	1.18	1.59	1.72	1.69	1.90	2.70	-	0.28	0.38	0.38	0.35
Aromatics	3.64	2.54	2.13	1.92	2.10	1.85	3.27	2.82	2.67	2.14	2.97	3.68	2.53	2.73	2.59	2.03
Alcohols	10.38	6.78	4.89	5.39	5.18	5.56	7.07	5.89	5.32	4.65	5.68	4.51	3.77	4.91	4.37	4.39
Aldehydes	1.74	1.43	1.54	1.71	1.86	1.85	2.54	2.23	2.17	2.39	2.40	2.60	1.29	2.09	2.16	2.33
Amides	0.25	0.57	1.22	0.66	1.21	0.68	0.62	0.44	0.38	0.30	0.47	0.75	0.51	0.56	0.69	1.18
Ketones	7.45	7.28	6.81	6.57	8.37	7.64	12.64	11.92	10.17	6.43	8.25	10.81	9.39	9.27	8.47	8.09
Esters	6.10	5.83	4.92	4.86	8.50	7.11	4.20	4.13	4.31	6.81	6.48	12.39	8.25	8.30	6.27	3.11
Furans	1.04	2.21	2.35	1.95	1.23	1.06	1.46	1.53	1.57	1.10	1.32	3.66	3.87	2.62	2.62	1.81
Guaiacols	1.02	1.31	1.55	1.75	2.20	2.71	1.30	1.27	1.46	1.52	2.02	-	0.66	1.31	1.54	2.19
Phenols	13.12	9.18	10.79	10.46	10.39	12.68	14.06	10.21	9.79	8.66	12.06	13.50	14.22	14.01	15.88	14.59
Carbohydrates	7.45	0.57	1.28	1.73	2.39	2.39	0.68	0.91	1.35	1.54	2.35	-	0.50	1.44	1.58	1.68

References

1. Jerzak, W.; Acha, E.; Li, B. Comprehensive Review of Biomass Pyrolysis: Conventional and Advanced Technologies, Reactor Designs, Product Compositions and Yields, and Techno-Economic Analysis. *Energies* **2024**, *17*, 5082. [CrossRef]
2. Naqvi, S.R.; Khoja, A.H.; Ali, I.; Naqvi, M.; Noor, T.; Ahmad, A.; Luque, R.; Amin, N.A.S. Recent progress in catalytic deoxygenation of biomass pyrolysis oil using microporous zeolites for green fuels production. *Fuel* **2023**, *333*, 126268. [CrossRef]
3. He, Q.; Huang, S.; Luo, W.; Su, Y.; Xia, M.; Zhou, N.; Zhou, Z. Study on the difference between in-situ and ex-situ catalytic pyrolysis of oily sludge. *Environ. Sci. Pollut. Res.* **2021**, *28*, 50500–50509. [CrossRef]
4. Kumar, R.; Strezov, V.; Lovell, E.; Kan, T.; Weldekidan, H.; He, J.; Jahan, S.; Dastjerdi, B.; Scott, J. Enhanced bio-oil deoxygenation activity by Cu/zeolite and Ni/zeolite catalysts in combined in-situ and ex-situ biomass pyrolysis. *J. Anal. Appl. Pyrolysis* **2019**, *140*, 148–160. [CrossRef]
5. Rahman, N.A.A.; Cardenas-Lizana, F.; Sanna, A. Lithium–Sodium Fly Ash-Derived Catalyst for the In Situ Partial Deoxygenation of *Isochrysis* sp Microalgae Bio-Oil. *Catalysts* **2023**, *13*, 1122. [CrossRef]
6. Fan, Y.; Yang, J.; Xu, A.; Li, X.; Cai, Y. In-situ catalytic pyrolysis of cellulose with lithium-ion battery ternary cathodes and ex-situ upgrading over Ru/HZSM-5 for bio-aromatics. *J. Anal. Appl. Pyrolysis* **2024**, *177*, 106373. [CrossRef]
7. Hubble, A.H.; Childs, B.A.; Pecchi, M.; Sudibyo, H.; Tester, J.W.; Goldfarb, J.L. Role of in situ (in contact with biomass) and ex situ (in contact with pyrolysis vapors) transition metal catalysts on pyrolysis of cherry pits. *Fuel* **2023**, *352*, 129062. [CrossRef]
8. Luan, P.; Chen, J.; Liu, T.; Wang, J.; Yan, B.; Li, N.; Cui, X.; Chen, G.; Cheng, Z. Ex-situ catalytic fast pyrolysis of waste polycarbonate for aromatic hydrocarbons: Utilizing HZSM-5/modified HZSM-5. *J. Anal. Appl. Pyrolysis* **2024**, *182*, 106667. [CrossRef]

9. Ruddy, D.A.; Schaidle, J.A.; Ferrell, J.R., III; Wang, J.; Moens, L.; Hensley, J.E. Recent advances in heterogeneous catalysts for bio-oil upgrading via "ex situ catalytic fast pyrolysis": Catalyst development through the study of model compounds. *Green Chem.* **2014**, *16*, 454–490. [CrossRef]
10. Xu, M.; Shi, Z.; Zhu, X.; Lai, Y.; Xia, A.; Huang, Y.; Jiang, X.; He, J.; Zhou, M.; Zhu, X.; et al. Ex-situ catalytic upgrading of biomass pyrolysis volatiles over thermal-decomposition products of spent lithium-ion batteries for bio-oil deoxygenation and hydrogen-rich syngas production. *Int. J. Hydrogen Energy* **2024**, *52*, 83–96. [CrossRef]
11. Liu, T.L.; Cao, J.-P.; Zhao, X.-Y.; Wang, J.-X.; Ren, X.-Y.; Fan, X.; Zhao, Y.-P.; Wei, X.-Y. In situ upgrading of Shengli lignite pyrolysis vapors over metal-loaded HZSM-5 catalyst. *Fuel Process. Technol.* **2017**, *160*, 19–26.
12. Cao, J.-P.; Li, L.-Y.; Morishita, K.; Xiao, X.-B.; Zhao, X.-Y.; Wei, X.-Y.; Takarada, T. Nitrogen transformations during fast pyrolysis of sewage sludge. *Fuel* **2013**, *104*, 1–6. [CrossRef]
13. Promsampao, N.; Chollacoop, N.; Pattiya, A. Regeneration of pristine HZSM-5 extrudates during the production of deeply deoxygenated bio-oil from ex situ catalytic fast pyrolysis of biomass in a bench-scale fluidised-bed reactor. *React. Chem. Eng.* **2022**, *7*, 398–415. [CrossRef]
14. HPrabhakara, M.; Bramer, E.A.; Brem, G. Hydrotalcite as a deoxygenation catalyst in fast pyrolysis of biomass for the production of high quality bio-oil. *J. Anal. Appl. Pyrolysis* **2022**, *161*, 105431. [CrossRef]
15. Li, Y.; Nishu; Yellezuome, D.; Li, C.; Liu, R. Deactivation mechanism and regeneration effect of bi-metallic Fe-Ni/ZSM-5 catalyst during biomass catalytic pyrolysis. *Fuel* **2022**, *312*, 122924. [CrossRef]
16. Abdulkareem-Alsultan, G.; Asikin-Mijan, N.; Obeas, L.K.; Yunus, R.; Razali, S.Z.; Islam, A.; Taufiq-Yap, Y.H. In-situ operando and ex-situ study on light hydrocarbon-like-diesel and catalyst deactivation kinetic and mechanism study during deoxygenation of sludge oil. *Chem. Eng. J.* **2022**, *429*, 132206. [CrossRef]
17. Mortensen, P.M.; Grunwaldt, J.-D.; Jensen, P.A.; Knudsen, K.G.; Jensen, A.D. A review of catalytic upgrading of bio-oil to engine fuels. *Appl. Catal. A Gen.* **2011**, *407*, 1–19. [CrossRef]
18. Cheng, S.; Wei, L.; Zhao, X.; Julson, J. Application, Deactivation, and Regeneration of Heterogeneous Catalysts in Bio-Oil Upgrading. *Catalysts* **2016**, *6*, 195. [CrossRef]
19. Furimsky, E.; Massoth, F.E. Deactivation of hydroprocessing catalysts. *Catal. Today* **1999**, *52*, 381–495. [CrossRef]
20. Mohabeer, C.; Abdelouahed, L.; Marcotte, S.; Taouk, B. Comparative analysis of pyrolytic liquid products of beech wood, flax shives and woody biomass components. *J. Anal. Appl. Pyrolysis* **2017**, *127*, 269–277. [CrossRef]
21. Mohabeer, C.; Reyes, L.; Abdelouahed, L.; Marcotte, S.; Taouk, B. Investigating catalytic de-oxygenation of cellulose, xylan and lignin bio-oils using HZSM-5 and Fe-HZSM-5. *J. Anal. Appl. Pyrolysis* **2019**, *137*, 118–127. [CrossRef]
22. Mohabeer, C.; Reyes, L.; Abdelouahed, L.; Buvat, J.-C.; Tidahy, L.; Abi-Aad, E.; Taouk, B. Production of liquid bio-fuel from catalytic de-oxygenation: Pyrolysis of beech wood and flax shives. *J. Fuel Chem. Technol.* **2019**, *47*, 153–166. [CrossRef]
23. HCerqueira, S.; Caeiro, G.; Costa, L.; Ribeiro, F.R. Deactivation of FCC catalysts. *J. Mol. Catal. A Chem.* **2008**, *292*, 1–13. [CrossRef]
24. Mukarakate, C.; Zhang, X.; Stanton, A.R.; Robichaud, D.J.; Ciesielski, P.N.; Malhotra, K.; Donohoe, B.; Gjersing, E.; Evans, R.J.; Heroux, D.S.; et al. Real-time monitoring of the deactivation of HZSM-5 during upgrading of pine pyrolysis vapors. *Green Chem.* **2014**, *16*, 1444–1461. [CrossRef]
25. Paasikallio, V.; Lindfors, C.; Kuoppala, E.; Solantausta, Y.; Oasmaa, A.; Lehto, J.; Lehtonen, J. Product quality and catalyst deactivation in a four day catalytic fast pyrolysis production run. *Green Chem.* **2014**, *16*, 3549. [CrossRef]
26. Vitolo, S.; Bresci, B.; Seggiani, M.; Gallo, M.G. Catalytic upgrading of pyrolytic oils over HZSM-5 zeolite: Behaviour of the catalyst when used in repeated upgrading–regenerating cycles. *Fuel* **2001**, *80*, 17–26. [CrossRef]
27. Charon, N.; Ponthus, J.; Espinat, D.; Broust, F.; Volle, G.; Valette, J.; Meier, D. Multi-technique characterization of fast pyrolysis oils. *J. Anal. Appl. Pyrolysis* **2015**, *116*, 18–26. [CrossRef]
28. Esbensen, K.H.; Guyot, D.; Westad, F.; Houmoller, L.P. *Multivariate Data Analysis: In Practice: An Introduction to Multivariate Data Analysis and Experimental Design*; CAMO Sosftware: Oslo, Norway, 2002.
29. Guizani, C.; Valin, S.; Billaud, J.; Peyrot, M.; Salvador, S. Biomass fast pyrolysis in a drop tube reactor for bio oil production: Experiments and modeling. *Fuel* **2017**, *207*, 71–84. [CrossRef]
30. Jahirul, M.I.; Rasul, M.G.; Chowdhury, A.A.; Ashwath, N. Biofuels Production through Biomass Pyrolysis—A Technological Review. *Energies* **2012**, *5*, 4952–5001. [CrossRef]
31. Ellens, C. Design, Optimization and Evaluation of a Free-Fall Biomass Fast Pyrolysis Reactor and Its Products. Master's Thesis, Iowa State University, Ames, IA, USA, 2009.
32. Choi, S.J.; Park, S.H.; Jeon, J.-K.; Lee, I.G.; Ryu, C.; Suh, D.J.; Park, Y.-K. Catalytic conversion of particle board over microporous catalysts. *Renew. Energy* **2013**, *54*, 105–110. [CrossRef]
33. Murata, K.; Liu, Y.; Inaba, M.; Takahara, I. Catalytic fast pyrolysis of jatropha wastes. *J. Anal. Appl. Pyrolysis* **2012**, *94*, 75–82. [CrossRef]
34. Park, H.J.; Dong, J.-I.; Jeon, J.-K.; Yoo, K.-S.; Yim, J.-H.; Sohn, J.M.; Park, Y.-K. Conversion of the Pyrolytic Vapor of Radiata Pine over Zeolites. *J. Ind. Eng. Chem.* **2007**, *13*, 182–189.
35. Park, H.J.; Park, Y.-K.; Kim, J.-S.; Jeon, J.-K.; Yoo, K.-S.; Yim, J.-H.; Jung, J.; Sohn, J.M. Bio-oil upgrading over Ga modified zeolites in a bubbling fluidized bed reactor. In *Studies in Surface Science and Catalysis*; Rhee, H.-K., Nam, I.-S., Park, J.M., Eds.; Elsevier: Amsterdam, The Netherlands, 2006; pp. 553–556.

36. Guo, Z.; Wang, S.; Zhu, Y.; Luo, Z.; Cen, K. Separation of acid compounds for refining biomass pyrolysis oil. *J. Fuel Chem. Technol.* **2009**, *37*, 49–52. [CrossRef]
37. Gayubo, A.G.; Aguayo, A.T.; Atutxa, A.; Aguado, R.; Olazar, M.; Bilbao, J. Transformation of Oxygenate Components of Biomass Pyrolysis Oil on a HZSM-5 Zeolite II Aldehydes, Ketones, and Acids. *Ind. Eng. Chem. Res.* **2004**, *43*, 2619–2626. [CrossRef]